CHEMISTRY OF MATERIALS

Article

pubs.acs.org/cm

Improved Performance of Solution-Processed n-Type Organic Field-Effect Transistors by Regulating the Intermolecular Interactions and Crystalline Domains on Macroscopic Scale

Suresh Vasimalla,[§] Satyaprasad P. Senanayak,[‡] Meenakshi Sharma,[§] K. S. Narayan,*[,‡] and Parameswar Krishnan Iyer*[,§,†]

[§]Department of Chemistry and [†]Centre for Nanotechnology, Indian Institute of Technology Guwahati, Guwahati 781039, Assam, India

[‡]Jawaharlal Nehru Centre for Advanced Scientific Research Jakkur, Bangalore 560064, India

Supporting Information

ABSTRACT: The development of four new n-channel naphthalene diimide (NDI) and perylene diimide (PDI) copolymers (NDI-Ph, NDI-BT, PDI-Ph, and PDI-BT) and their solution processed thin film transistor (TFT) devices are reported. Remarkable enhancements in the electron transport behavior for all the four copolymers were achieved on improving the intermolecular interactions in their thin film structures. These solution processable n-type copolymers having NDI and PDI backbone were synthesized in high yields (83−86%) by palladium catalyzed Suzuki coupling reactions, and their excellent solubility in several organic solvents allowed their deposition in organic thin film transistor (OTFT) devices from solution directly. Since these copolymers possess crystalline domains, annealing their films induced crystalline phases in the thin film structures with a very high degree of enhancement in crystallinity that was more prominent for PDI copolymers as compared to NDI derivatives. This resulted in significant enhancement in the intermolecular interactions in the thin film state on the macro scale, facilitating improved and higher charge carrier transport in annealed devices as compared to the as-spun devices that have lesser crystalline phases. The transport measurements performed for these four copolymers helped us to understand the difference in transport mechanism between D−A and A−A moiety and confirmed that tuning the thin film structures and the electronic properties by modifying the copolymer backbone structures as well as annealing them at appropriate temperature has profound implications on the level of improvement in electron transport behavior. The enhancement in μ_e values for all four copolymers is very large for any reported n-type copolymers. It is observed that the extended conjugation in the four copolymer structures, the efficient intermolecular interactions in the thin film state, and the formation of crystalline domains in the copolymers after annealing are, in principle, responsible for the enhanced device performance. These copolymers demonstrated electron mobility enhancement of several orders and are reported to be as high as 0.8 $cm^2\ V^{-1}\ s^{-1}$ and 0.2 $cm^2\ V^{-1}\ s^{-1}$ with I_{on}/I_{off} ratios 10^5 for NDI-Ph and NDI-BT, while those of PDI-Ph and PDI-BT are 0.04 $cm^2\ V^{-1}\ s^{-1}$ and 0.032 $cm^2\ V^{-1}\ s^{-1}$, respectively, with I_{on}/I_{off} ratios of 10^3−10^4.

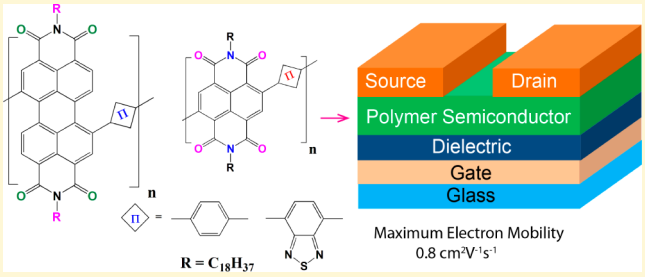

INTRODUCTION

Polymer field effect transistors (PFETs) have attracted significant interest during the past several years because they have contributed significantly in the fabrication of low cost organic optoelectronic devices such as p−n junctions,[1,2] photovoltaic cells,[3,4] complementary circuits,[5] and driving organic light emitting diodes (OLED) for flexible display.[6,7] All these applications require both hole transporting (p-type) and electron transporting (n-type) materials with suitable physical, chemical, electrical, and photochemical properties. The n-type materials development has lagged behind the p-type materials over the years since the majority of studies reported so far have focused on p-type semiconductor materials and devices.[8,9] In recent years, few reports on the development of ambipolar[10,11] and n-type semiconductors with encouraging performances have appeared.[12,13] For the electronics industries that rely on organic materials, development of low-cost solution processable n-type semiconducting materials with high performance remains a challenge. One of the major drawbacks with n-type materials is their instability at ambient conditions. In this regard, we demonstrate n-type PFETs with electron mobilities ∼1 $cm^2\ V^{-1}\ s^{-1}$ which are relatively stable under ambient conditions and could be aligned to improve the transport properties by several orders.

There are numerous building blocks being developed to fabricate air stable n-channel semiconducting materials, while

Received: May 17, 2014
Revised: June 13, 2014
Published: June 18, 2014

   dx.doi.org/10.1021/cm501780p | Chem. Mater. 2014, 26, 4030−4037

rylene based polymers, especially naphthalene,[14,15] perylene,[16,17] and pyromellitic tetracarboxylic diimides[18,19] are the most promising. Naphthalene (NDI) and perylene diimides (PDI) possess aromatic planar conjugated structure and are favorable for good charge transport with performances comparable to p-type semiconducting materials. These classes of materials have an excellent combination of thermal, optical, redox, and electrical properties as well as very high moisture and oxygen resistance.[20] The functionalization at the diimide position with aliphatic alkyl chain, either branched or long chain, provides good solubility in common organic solvents, enhancing their processability.[21] Additionally, the possibility to obtain interdigitated structures limits the percolation of moisture to the conjugated core, thereby making it stable for ambient performance.[22] Many NDI and PDI based small molecules[23,24] and oligomers[25,26] have been reported with self-assembling properties and good charge transporting ability. Few newly developed materials showing high electron mobility include: ladder type naphthalene,[27] perylene diimide,[28] and D−A type copolymers of NDI, PDI with thiophene,[29,30] bithiophene,[31] dithienothiophene,[32] phenothiazine,[33] dithienopyrrole,[34] and phenylene.[35] High electron mobility of up to 0.45−0.85 $cm^2 V^{-1} s^{-1}$ was reported with NDI/PDI derivative and bithiophene copolymers[36] and NDI−vinylene−thiophene copolymers which exhibited mobilities of up to 1.8 $cm^2 V^{-1} s^{-1}$.[37] In PDI based copolymer, electron mobilities of up to 0.075 $cm^2 V^{-1} s^{-1}$ have been possible with the dithienothiophene unit,[38] and with liquid crystalline copolymers.[39,40]

Despite these efforts it remains unclear why D−A based NDI and PDI copolymers have better μ_{FET}. In addition, the role of anisotropic properties, improving the structural order in solution-processed n-type polymers, and the enhanced film morphology on the macroscopic scale are also very crucial for obtaining high-performance OFETs. In this manuscript, we have synthesized four (thiophene-free) copolymers based on phenyl and/or benzothiadiazole as copolymerizing units with linear C18 substituted NDI and PDI derivatives in order to gain a relatively higher understanding on the roles and features of different D−A and A−A structures and carefully study the transport behavior in these polymers. We also demonstrate that enhancing the polymer anisotropic properties by annealing at appropriate temperature significantly improves the intermolecular interactions as well as the formation of crystalline domains on the macroscopic scale, facilitating large enhancement in charge carrier transport. Since conjugated polymers inherently possess anisotropic characteristics, they can be realized in device applications only when these conjugated chains are aligned in such a manner that the crystallites do not remain entrenched within the amorphous polymer phases. Tuning the thin film structures of the polymers by annealing facilitates the conjugated chains alignment over larger macrodomains and enhances the structure−property relationships by demonstrating highly improved charged transport behavior here. Hence, developing processing strategies in these materials to overcome the amorphous domains and recognizing the importance of conjugated backbone macrostructure chain alignment are, in principle, extremely crucial for device improvements.

EXPERIMENTAL SECTION

Materials and Characterization. Perylene tetracarboxylic dianhydride, naphthalene tetracarboxylic dianhydride, 1,4-benzene diboronic acid, and 2,1,3-benzothiadiazole-4,7-bis(boronic acid pinacol ester) were purchased from Sigma-Aldrich and were used without further purification. The dielectric material hydroxyl free divinyltetramethylsiloxanebis-benzocyclobutene (BCB) is obtained from Dow Chemicals. 2,6-Dibromo naphthalene tetracarboxylic dianhydride (NTCDA-Br_2[41] and 1,7-dibromo-3,4:9,10-perylene teracarboxylic dianhydride (PTCDA-Br_2), *N*,*N*′-bis(octadecyl)-1,7-dibromo-3,4:9,10-perylenetetracarboxylicdianhydride, and *N*,*N*′-bis(octadecyl)-2,6-dibromonaphthalene-1,4,5,8-tetracarboxylic dianhydride were synthesized following the published literature procedure (Scheme 1).[31] All

Scheme 1. Synthesis of Monomers and Copolymers[a]

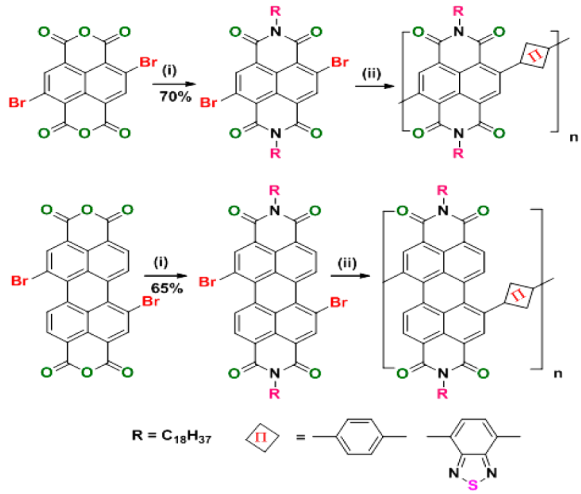

[a](i) *o*-Xylene, propionic acid, *n*-octadecylamine, 140 °C, 6 h; (ii) $Pd(PPh_3)_4$, K_2CO_3, 2:1 mixture of THF/H_2O, aliquat, 80 °C, 36 h, 1,4-benzene diboronic acid, or 2,1,3-benzothiadiazole-4,7-bis(boronic acid pinacol ester).

the polymers were synthesized by Suzuki coupling reaction. ^1H NMR and ^{13}C NMR were recorded on Varian AS 400 MHz and Bruker 600 MHz NMR spectrometers. MALDI-TOF-MS experiments were done on AB SCIEX, U.S.A., instrument with a4800 plus MALDI TOF/TOF Analyzer. Elemental analysis was done on CHNS Analyzer, PerkinElmer, 2400 (U.S.A.). UV−vis spectra were recorded on a PerkinElmer Model Lambda-25 spectrophotometer. Photoluminescence spectra were recorded on Varian Cary Eclipse spectrophotometer. Electrochemical measurements were carried out under argon on a deoxygenated solution of tetra *n*-butyl ammonium perchlorate (0.1M) in acetonitrile using a CH instruments Model 700D series Electrochemical workstation. A glassy carbon as working electrode, platinum wire as counter electrode, and Ag/Ag^+ as reference electrodes were used. Thermogravimetric analysis (TGA) was performed on Mettler Toledo, model TG/SDTA 851 e, thermogravimetric analyzer under a nitrogen flow at a heating rate of 10 °C/min. Differential scanning calorimetry was done on a Mettler Toledo, Model DSC 1, Stare system. The gel permeation chromatography measurements were performed on a waters 515 chromatograph connected to waters 2414 refractive index detector using THF as eluent and polystyrene standards as calibrants. AFM images were taken by an Agilent 5500-STM instrument, and FESEM images were recorded in a Sigma Carl ZEISS scanning electron microscope. XRD analyses were done by Bruker D8 Discover Diffractometer. A Leica polarizable optical microscope was used to study the anisotropic morphology of the copolymer films.

Preparation of Films for AFM, FESEM, XRD, and POM. The copolymers were spin coated on glass substrates at 500 rpm for 2 min and then heated for 30 min at 50 °C to evaporate the solvent. FESEM images were recorded with these films. Similarly, AFM images of the films were recorded for as-spun and annealed (30 min at 150 °C) films. For XRD measurement the films were prepared under the same conditions as followed for the device fabrication. For POM studies, the copolymers were dissolved in chloroform and drop-casted on a glass

dx.doi.org/10.1021/cm501780p | Chem. Mater. 2014, 26, 4030−4037

Table 1. GPC Characterization and % Yields of Polymers, Electrochemical and Optical Band Gaps, and Thermal Data

polymer	M_n[a] (Da)	M_w[a] (Da)	PDI[a] (yield %)	HOMO[b] (eV)	LUMO[b] (eV)	E_g[c] (eV)	E_g[d] (eV)	T_d (°C)
NDI-Ph	6811	13579	1.99 (84%)	−5.173	−3.15	2.02	1.55	341
NDI-BT	5171	6627	1.74 (85%)	−5.14	−3.03	2.10	1.72	350
PDI-Ph	16082	24657	1.53 (83%)	−5.89	−3.49	2.40	1.57	363
PDI-BT	30619	35739	1.16 (86%)	−5.49	−3.08	2.41	1.59	385

[a]M_n, M_w, number-average and weight-average molecular weights, and PDI, polydispersity index, are obtained from GPC. [b]HOMO and LUMO estimated from the onset oxidation and reduction potentials, respectively, assuming the absolute energy level of ferrocene/ferrocenium couple to be 4.8 eV below vacuum. [c]HOMO−LUMO gap estimated by electrochemistry. [d]Optical band gap calculated from absorption. T_d: degradation temperature by TGA.

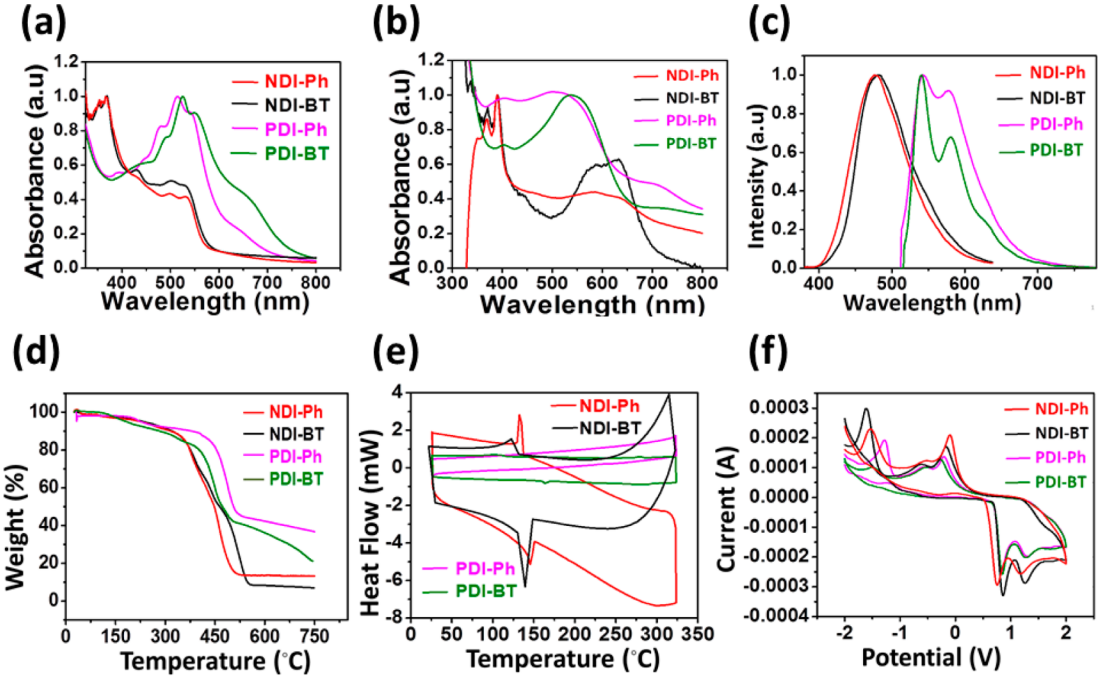

Figure 1. (a) UV−vis spectra in THF (10^{-5} M), (b) UV−vis spectra in thin films (~50−60 nm), (c) PL spectra in THF (10^{-5} M) of polymers. (d) TGA chromatograms carried out at a rate of 5 °C/min. (e) DSC chromatograms of the second cycle of the polymers carried out at a rate 5 °C/min under nitrogen atmosphere. (f) Cyclic voltammograms of the drop casted polymer films (~100 nm) on carbon working electrode performed at a scan rate of 0.5 mV/s in 0.1 M TBAP in acetonitrile under argon atmosphere.

slide and heated for 2 h at 50 °C to remove residual solvent. During the POM annealing experiments the films were heated from 50 to 180 °C at a rate of 5 °C/min and then cooled to 50 °C at the same rate, and the images were recorded at 50× resolution.

Device Fabrication and Characterization. Detailed transport study of the NDI and PDI copolymers was performed using bottom gate top contact FET geometry. For device fabrication, Al metal is coated as the gate electrode by physical vapor deposition (10^{-6} mbar, 40 nm thick) on RCA cleaned glass substrate. Dielectric layer hydroxyl free divinyltetramethylsiloxane bis-benzocyclobutene (BCB) is then coated at 1000 rpm for 1 min and annealed in N_2 filled glovebox atmosphere at 290 °C. The resultant dielectric layer had a $C_i \sim 4$ nF/cm^2 measured directly using the C−V meter inbuilt in Keithley 4200 semiconductor parameter analyzer. Typical dielectric thickness is estimated to be around 0.5−0.6 μm as measured using Filmetrics (F20—EXR) thickness measurement setup. The surface of the dielectric was coated (1500 rpm for 30 s) with a thin monolayer of hexamethyldisilazane (HMDS) and annealed at 110 °C for 2 h. The copolymer layer is then introduced from the solution phase (15 mg/mL in THF) by spin coating at 1000 rpm for 1 min and annealed at different temperatures (110−150) °C for 30 min to optimize the performance. In order to facilitate electron injection Al source-drain electrodes were then coated (10^{-6} mbar, 40 nm thick) to complete the device fabrication. We observe an injection limited response with lower μ_{FET} for Au S-D electrodes. The device characterizations were performed using standard Keithley 4200 semiconductor characterization systems and cross-checked with measurement using Keithley 2400 Source meters and high-impedance Keithley 6514 electrometer. Typical FET performance is estimated from average characteristics of five to seven devices.

RESULTS AND DISCUSSION

Synthesis and Characterization. The syntheses of four new conjugated copolymers were achieved in 83−86% yields (Scheme 1). The synthesis details of the monomers and copolymers are reported in the Supporting Information. The Suzuki coupling reaction of dibrominated NDI and PDI derivatives with benzene-1,4-diboronic acid and 2,1,3-benzothiadiazole bisboronic ester resulted in the formation of NDI-Ph, NDI-BT, PDI-Ph, and PDI-BT copolymers. All the monomers and polymers were well-characterized by NMR (Supporting Information Figures S1−S2, S4−S9, and S11−S14), MALDI (Supporting Information Figure S3 and S10)/gel permeation chromatography (GPC), elemental analysis, DSC, TGA, PL, UV−vis, and cyclic voltammetry and their morphologies studied by AFM, FESEM, POM, and XRD techniques (Figure 2), (Supporting Information Figure S15). The TGA analysis reveals that the copolymers are stable up to

dx.doi.org/10.1021/cm501780p | Chem. Mater. 2014, 26, 4030−4037

350 °C. These polymers were fabricated and tested for solution processable polymer field effect transistors (PFETs). It was observed that these NDI and PDI derivatives exhibit field effect electron mobilities (μ_{FET}) that are as high as 0.8 cm^2 V^{-1} s^{-1}(NDI-Ph), 0.2 cm^2 V^{-1} s^{-1}(NDI-BT), 0.04 cm^2 V^{-1} s^{-1} (PDI-Ph), and 0.032 cm^2 V^{-1} s^{-1} (PDI-BT) with a current modulation in the range of 10^4−10^5. High μ_{FET} can be attributed to the enhanced π−π stacking originating from the intermolecular overlap of the D−A orbitals. Table 1 represents their molecular weight and polydispersity index (PDI) as obtained from GPC in THF (polystyrene standard). Due to the presence of alkyl chains all four copolymers were readily soluble in common organic solvents such as toluene, THF, chloroform, dichloromethane, chlorobenzene, and xylenes and could be solution processed onto desired substrates for achieving smooth films.

Photophysical Properties. To understand the aggregation mechanism, the UV−visible spectra of the copolymers were studied in THF at a concentration of 10^{-5} M. NDI-BT shows absorption peaks at 360, 371, and 449 nm, which are assigned to basic naphthalene diimide core transitions while the peak at 538 nm is due to general polymer aggregation. Another peak observed at 438 nm is generally observed for the benzothiadiazole moiety. NDI-Ph shows peaks at 360 nm and 370 nm which are assigned to the basic naphthalene core transitions and a peak of polymer aggregation at 540 nm. The PDI-BT gives absorption bands at 550 nm, 525 nm, and 489 nm and those of PDI-Ph are at 548 nm, 513 nm, and 485 nm which are assigned to the general PDI based (S_o−S_o, S_o−S_1, S_o−S_2) transitions (Figure 1a).[42]The absorption spectra of the spin coated polymer films on glass (Figure 1b) show a red shift in the peaks for all the copolymers as compared to the solution state absorption peaks. For NDI-BT copolymer the 538 nm peak was significantly red-shifted to around 625 nm with similar red shift of up to 371, 391, and 449 nm from the initial positions of 360, 371, and 438 nm, respectively. Similarly, the 540 nm peak of the NDI-Ph copolymer was shifted to 600 nm caused by the strong polymer interchain interaction. The other peaks observed at 360 nm and 370 nm for NDI-Ph are also shifted to 370 nm and 390 nm in thin films as compared to the solution spectra. The shoulders at 675 nm in PDI-BT and 660 nm in PDI-Ph which are assigned to π−π polymer interactions are observed to be shifted to 739 and 721 nm, respectively, in thin films indicating the general polymer aggregation in solid state. All other peaks of PDI-BT are also found to be red-shifted. The optical band gaps calculated from the absorption edge for NDI-Ph and NDI-BT were found to be 1.55 eV and 1.72 eV and those of PDI-BT, PDI-Ph copolymers are 1.57 and 1.59 eV, respectively (Table 1). PL spectroscopy measurements of polymers were performed in dilute 10^{-5} M THF solutions. The NDI-BT copolymer shows an emission peak at 480 nm which corresponds to the main absorption peak at 371 nm of the naphthalene core transition. NDI-Ph polymer exhibits an emission peak at around 472 nm corresponding to that of 370 nm in the absorption spectra. The PDI-BT polymer shows emission peaks at 537 nm and 577 nm corresponding to 525 nm and 550 nm peaks in UV (Figure 1c). PDI-Ph polymer gives emission peaks at 538 and 575 nm corresponding to 513 and 548 nm absorption peaks in THF.

Thermal Properties. The thermal properties of the polymers were studied by thermogravimetric analysis (TGA) and differential scanning calorimeter (DSC). TGA analysis was done in the range 25−800 °C at a rate of 5 °C/min under nitrogen flow. All the polymers were very stable, and their onset degrading temperatures were found to be in the range of 341−385 °C (Figure 1d). The onset thermal degradation temperatures of all the polymers are shown in Table 1. In DSC, the polymers were heated from 25 to 325 °C and then again cooled to 25 °C with a rate of 5 °C/min for three cycles under nitrogen flow. The chromatograms of the second cycle are shown in Figure 1e. NDI-Ph copolymer shows an endothermic peak at 145 °C in the second heating cycle and an exothermic peak at 132 °C in the second cooling cycle which indicates the melting and crystalline temperatures of the polymer, respectively. Similarly, NDI-BT copolymer shows an endothermic peak at 142 °C and an exothermic peak at 125 °C in the second heating and cooling cycles corresponding to the melting and crystalline temperatures respectively showing that both polymers are crystalline in nature.

The PDI-Ph copolymer did not undergo any change during the heating or cooling process. The PDI-BT copolymer shows an endothermic peak at 164 °C during heating which corresponds to melting and exothermic peak of crystallization at 110 °C during cooling process, which indicates the crystalline behavior of the copolymer. Hence, the DSC reveals that NDI-Ph, NDI-BT, and PDI-BT copolymers possess crystalline domains within their structures.

Electrochemical Properties. To estimate the HOMO and LUMO energy levels of the copolymers, cyclic voltammetry (CV) was performed. The copolymers were drop casted on carbon working electrode. Silver as the reference electrode and platinum wire as the counter electrode were used in these experiments. The HOMO and LUMO levels were estimated by the onset oxidation and onset reduction peaks assuming the absolute energy level of the ferrocene/ferrocenium couple to be 4.8 eV below vacuum. 0.1 M tetrabutylammonium perchlorate (TBAP) as electrolyte in deoxygenated acetonitrile and ferrocene as standard were used in argon atmosphere. The HOMO/LUMO energies were calculated by substituting the onset reduction and onset oxidation peak values in E_{LUMO} = $[(E_{red} - E_{1/2}(\text{ferrocene})) + 4.8]$ eV, E_{HOMO} = $[(E_{ox} - E_{1/2}(\text{ferrocene})) + 4.8]$ eV. The LUMO levels of NDI-BT, NDI-Ph, PDI-BT, and PDI-Ph are −3.03 eV, −3.15 eV, −3.49 eV, and −3.08 eV, respectively. Similarly HOMO levels of the copolymers NDI-BT, NDI-Ph, PDI-BT, and PDI-Ph calculated from CV are −5.14 eV, −5.173 eV, −5.89 eV, and −5.49 eV, respectively (Figure 1f). The energy levels and band gaps calculated from cyclic voltammetry of thin films are represented in Table 1

Morphology Characterization. Polymer thin films were characterized by AFM, FESEM, XRD, and polarized optical microscopy (POM) to obtain further information on crystallinity and morphology which is relevant for device characterization. Out-of plane XRD measurements were performed on thin films of the NDI and PDI copolymers (Figure 2) to obtain information regarding the molecular reorganization. As-spun polymeric films reveal π−π stacking in the range of 4.02−4.18 Å and a broad primary diffraction peaks at 2θ = 4.09−4.34° corresponding to the *d*-spacing values of 18.51−27.84 Å. Annealing of the thin films reduced the *d*-spacing to a range of 18.26−24.65 Å and π−π stacking distance to 4.0−4.16 Å. This indicates that denser interdigitated lamellar packing is obtained by annealing the polymer films, which is an inherent anisotropic characteristic of conjugated backbone possessing polymers. It should be noted that these magnitudes of *d*-spacing and π−π stacking obtained in these polymers are

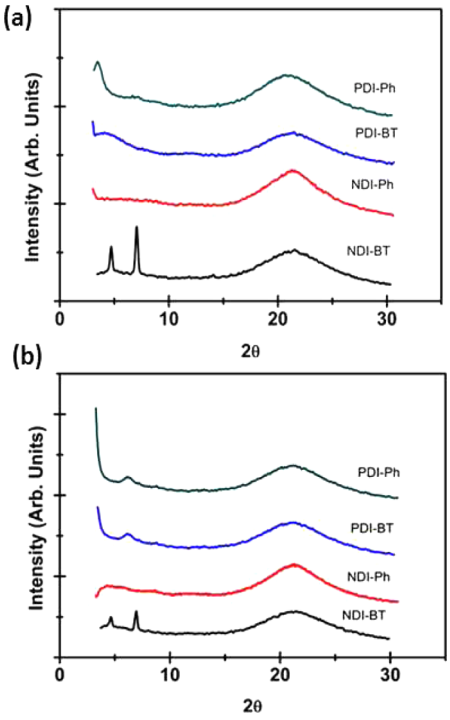

Figure 2. Out of plane X-ray diffraction patterns of (a) as-spun and (b) annealed (150 °C) copolymer films.

relatively lower than other nonthiophene based NDI polymers reported[35] which gets reflected in the enhanced transport properties. In addition, annealing the polymer films decreases the fwhm of the peaks (Table S1 in Supporting Information) corresponding to $\pi-\pi$ stacking as well as the *d*-spacing pointing to the enhanced morphological ordering with annealing.

AFM imaging was carried out on optical quality films coated under similar condition as those used in device studies. AFM images for as-spun films do not exhibit any crystallite formation (Figure 3a,c,e,g). However, it was observed that annealing the thin films at 150 °C introduces crystallites in the film (Figure 3b,d,f,h). This trend is consistent with DSC measurement which shows crystallization at ∼150 °C. It should be noted that the degree of enhancement of crystallinity is more prominent for PDI films compared to NDI copolymer films. This was substantiated from observations of a larger number of crystallites obtained in case of PDI-Ph and PDI-BT compared to NDI-Ph and NDI-BT. Furthermore, FE-SEM measurements were also performed on these copolymers to examine the thin film microstructure. FE-SEM images show interconnected crystalline fibrillar network of the copolymers which supports enhanced transport, weakly affected by defects.[43,44] In addition, POM studies performed on films of the these four copolymers confirmed the appearance of macroscale crystalline domains after annealing above 150 °C (Figure 4) due to their inherent structural anisotropic. These features can be directly correlated to large enhancement of μ_{FET} upon thermal annealing in PDI derivatives as compared to the NDI derivatives.

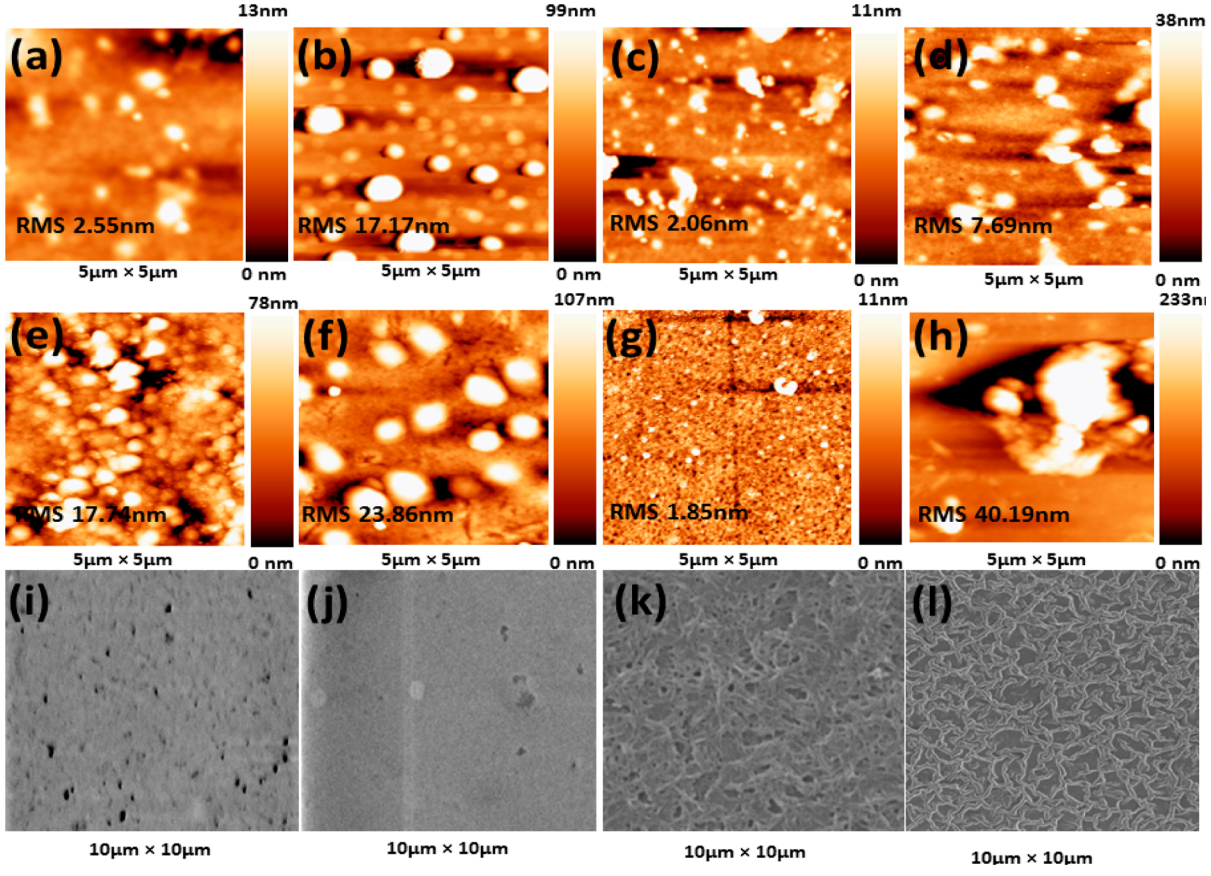

Figure 3. AFM topography image (5 μm × 5 μm) for the copolymer films: NDI-Ph (a) as-spun and (b) annealed; NDI-BT (c) as-spun and (d) annealed; PDI-Ph (e) as-spun and (f) annealed; PDI-BT (g) as-spun and (h) annealed. Typical FE-SEM images (10 μm × 10 μm) of (i) NDI-Ph, (j) NDI-BT, (k) PDI-Ph, and (l) PDI-BT films.

dx.doi.org/10.1021/cm501780p | *Chem. Mater.* 2014, 26, 4030−4037

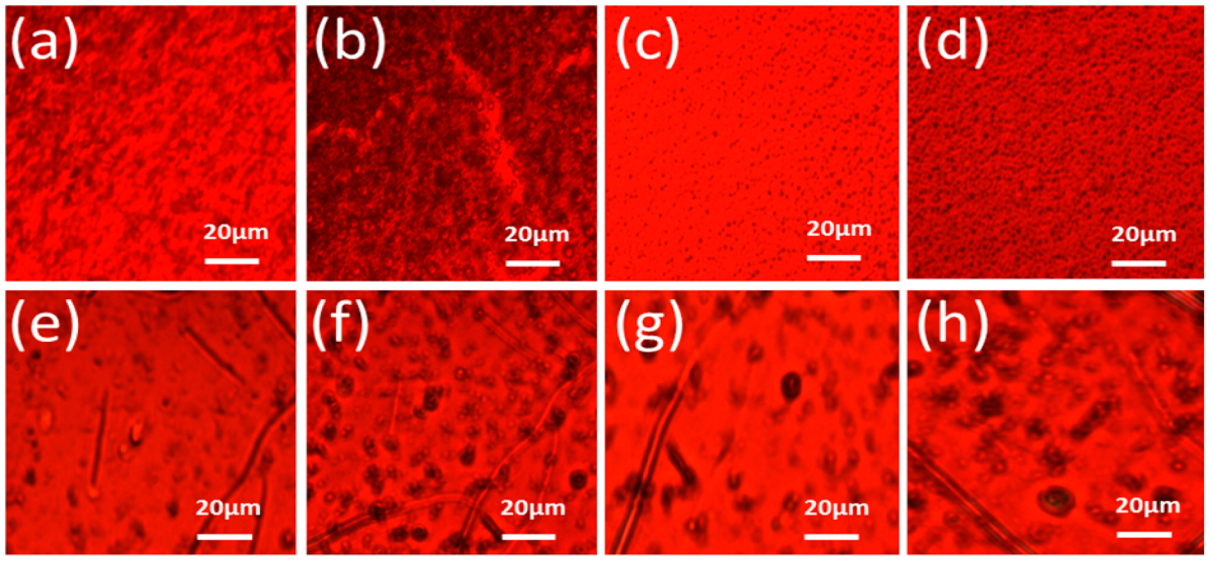

Figure 4. Polarizable optical microscope images of (a) NDI-Ph before annealing and (b) after annealing, (c) NDI-BT before annealing and (d) after annealing, (e) PDI-Ph before annealing and (f) after annealing, and (g) PDI-BT before annealing and (h) after annealing.

FET Measurements. Top contact bottom gated FETs were fabricated with all the copolymers in the procedure as described in the Experimental Section. The devices demonstrated well-defined linear and saturation behavior with electron only mobility and ON/OFF ratio exceeding 10^4 (Figure 5, Supporting Information Figure S16). A typical plot showing FET characteristics measured under inert conditions is shown in Figure 5. Similar FET characteristic with lower μ_{FET} is obtained when the devices are operated under ambient conditions (Supporting Information Figure S17). Although molecules with phenylene substitution are of D−A type, hole transport was not observed even with Au S-D electrodes. This feature can be attributed to weaker electron donating ability of the phenylene group. NDI-Ph showed the highest electron μ_{FET} ~ 0.8 $cm^2\ V^{-1}\ s^{-1}$ whereas FETs fabricated with NDI-BT had μ_{FET} ~ 0.2 $cm^2\ V^{-1}\ s^{-1}$ after annealing at 150 °C. The PDI derivatives, PDI-Ph and PDI-BT, also demonstrated μ_{FET} ~ 0.04 $cm^2\ V^{-1}\ s^{-1}$ and 0.032 $cm^2\ V^{-1}\ s^{-1}$ respectively, upon annealing up to 150 °C. Annealing increases the μ_{FET} by several orders, which are among the highest enhancement values for NDI and PDI based copolymers (Table 2). The observed enhancement of μ_{FET} is consistent with the occurrence of crystallites with annealing in the microscopic images and a crystalline transition temperature in DSC. In addition, XRD measurements on these thin films also indicate a decrease in *d*-spacing and $\pi-\pi$ stacking distance with annealing for all the polymers. Specifically, it was also observed that with annealing the decrease in *d*-spacing and $\pi-\pi$ stacking distance is higher for benzothiadiazole based molecules compared to phenylene substituted copolymers which corroborates with a larger change in the μ_{FET}.

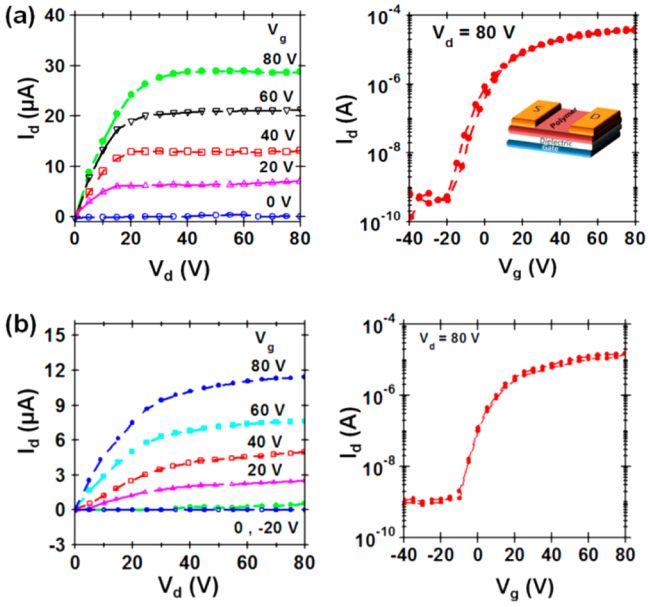

Figure 5. Typical output and transconductance characteristics for FETs fabricated under vacuum with (a and b) NDI-Ph and (c and d) PDI-Ph active layer and BCB as the dielectric (C_i ~ 2−4 nF/cm^2). Typical device dimensions are $W \approx 1$ mm and $L \approx 60-100$ μm. Inset (top) shows the schematic of the device.

Table 2. Performance Parameters of OFETs Obtained under Different Annealing Conditions

polymers	annealing temperature (°C)	average μ_{FET} ($cm^2\ V^{-1}\ s^{-1}$)	maximum μ_{FET} ($cm^2\ V^{-1}\ s^{-1}$)	I_{on}/I_{off}
NDI-Ph	as-spun	0.1	0.8	~ 10^5
	110	0.4		
	150	0.6		
NDI-BT	as-spun	0.007	0.2	>10^4
	110	0.05		
	150	0.08		
PDI-Ph	as-spun	0.005	0.04	>10^4
	110	0.008		
	150	0.015		
PDI-BT	as-spun	0.001	0.032	>10^4
	110	0.004		
	150	0.01		

Upon comparing the NDI and PDI derivatives, it is evident that the NDI derivatives exhibit μ_{FET} values which are at least

dx.doi.org/10.1021/cm501780p | *Chem. Mater.* 2014, 26, 4030−4037

an order of magnitude higher than the corresponding PDI derivatives. This can be attributed to the enhanced interdigitated lamellar packing and better $\pi-\pi$ stacking in NDI polymers. Annealed films of NDI polymers exhibit *d*-spacing in the range of 18.26−19.82 Å compared to 21.00−24.65 Å for PDI based polymers. Similarly, the $\pi-\pi$ stacking distance increases from 4.06 Å in NDI-Ph to 4.16 Å in PDI-Ph polymer (Table 3).

Table 3. Summary of Variation in $\pi-\pi$ Stacking and *d* Spacing of the Polymers

		as-cast films		annealed films	
polymers	(00*n*)	2θ	*d* (00*n*) spacing (Å)	2θ	*d* (00*n*) spacing (Å)
NDI-Ph	(001)	4.33	19.85	4.34	19.82
	(002)	-	-	-	-
	$\pi-\pi$	21.25	4.07	21.27	4.06
NDI-BT	(001)	4.65	18.51	4.71	18.26
	(002)	-	-	-	-
	$\pi-\pi$	21.48	4.02	21.58	4.00
PDI-Ph	(001)	-	-	-	-
	(002)	6.64	25.91	6.66	25.81
	$\pi-\pi$	20.84	4.14	20.97	4.12
PDI-BT	(001)	-	-	-	-
	(002)	6.12	28.11	6.14	28.02
	$\pi-\pi$	21.06	4.10	21.05	4.10

Importantly, the observed μ_{FET} values are higher than those of other nonthiophene based NDI polymers and are comparable to NDIOD-T2.[36,45] A plot of FET characteristics obtained under similar conditions at our laboratory with NDIOD-T2 is shown in Supporting Information Figure S16c. This comparable μFET can be attributed to a combination of factors, ranging from the molecular level to an optimum dielectric-semiconductor interface. The presence of linear alkyl chains in NDI-Ph and NDI-BT polymer improves the polymer packing and the $\pi-\pi$ stacking. In comparison to the typical *d*-spacing of 23−24 Å observed for nonthiophene based NDI the *d*-spacings in these NDI polymer films were obtained as 18.26−19.82 Å,[35] indicating better lamellar structure and closely packed interdigitated structure. In addition, the $\pi-\pi$ stacking distance of the NDI copolymers is in the range of 4.00−4.06 Å which is comparable to NDIOD-T2 (3.93 Å)[46] and better than other nonthiophene based NDI molecules (4.51 Å).[35] Hence, these molecules have a higher propensity to form ordered crystallites and interconnected aggregates on the macroscopic scale which supports enhanced transport as observed for other high mobility polymers reported recently.[43,47] Another interesting observation in the transport measurement is the enhanced performance of the D−A type molecules (NDI-Ph or PDI-Ph) compared to A−A type (NDI-BT or PDI-BT molecule). This indicates the apparent importance of the intermolecular D−A type interaction on the charge transport compared to the geometry and microstructure of the molecule which can be a general way to achieve high mobility in NDI or PDI polymeric materials.

CONCLUSIONS

In summary, we demonstrated the importance of the correlation between the conjugated backbone macrostructure, linear alkyl chains, and anisotropy behavior in spin-coated aligned thin films of perylene diimide and naphthalene diimide copolymers. The thin film structures and electronic anisotropic properties in conjugated copolymers can be regulated, which results in efficient intermolecular interactions, polymer packing, $\pi-\pi$ stacking, and the formation of crystalline domains over large area after annealing, thereby facilitating large enhancement in charge carrier transport. The optical, thermal, and redox characterization of the copolymers indicates good polymeric aggregates, high thermal stability with the tendency to form crystalline domains, and suitable energetics which support efficient electron injection. This was further supported by the morphology patterns observed in the AFM, FESEM, and POM images. The transport studies performed under different annealing conditions up to 150 °C demonstrated huge enhancement in electron μ_{FET} with maximum values of 0.8 $cm^2\ V^{-1}\ s^{-1}$ for the NDI-Ph and 0.04 $cm^2\ V^{-1}\ s^{-1}$ for the PDI-Ph polymers. The extended conjugation and efficient intermolecular interactions observed in thin films, along with the formation of crystalline domains as also confirmed by DSC analysis after annealing are collectively responsible for the enhanced device characteristics. This study conclusively illustrates that D−A copolymers display better properties compared to A−A copolymers and demonstrates a route to develop high-performing, solution processable copolymers.

ASSOCIATED CONTENT

Supporting Information

The synthesis and characterization of the monomers and four copolymers and scanned NMR and MALDI mass spectra are included. The typical output and transconductance characteristics with BT copolymers are also mentioned. This material is available free of charge via the Internet at http://pubs.acs.org.

AUTHOR INFORMATION

Corresponding Authors

*E-mail: pki@iitg.ernet.in (P.K.I.).
*E-mail: narayan@jncasr.ac.in (K.S.N.).

Notes

The authors declare no competing financial interests.

ACKNOWLEDGMENTS

The authors thank the Department of Science and Technology (DST), India (Nos. DST/TSG/PT/2009/11, DST/TSG/PT/2009/23, DST/SB/S1/PC-020/2014), and IGSTC/MPG/PG(PKI)/2011A/48 for financial support. The Central Instruments Facility, IIT Guwahati, is acknowledged for microscopy and spectroscopy facilities. We thank Prof. S. S. Ghosh, IIT Guwahati, for MALDI analysis and Dr. N. H. Khan, CSMCRI, India, for elemental analysis. S.P.S. acknowledges CSIR India for a fellowship.

REFERENCES

(1) Cheng, C. H. W.; Lonergan, M. C. *J. Am. Chem. Soc.* **2004**, *126*, 10536−10537.
(2) Robinson, S. G.; Lonergan, M. C. *J. Phys. Chem. C* **2013**, *117*, 1600−1610.
(3) Zhou, E. J.; Cong, J. Z.; Zhao, M. X.; Zhang, L. Z.; Hashimoto, K.; Tajima, K. *Chem. Commun.* **2012**, *48*, 5283−5285.
(4) Zhang, Q. L.; Cirpan, A.; Russell, T. P.; Emrick, T. *Macromolecules* **2009**, *42*, 1079−1082.
(5) Baeg, K. J.; Kim, J.; Khim, D.; Caironi, M.; Kim, D. Y.; You, I. K.; Quinn, J. R.; Facchetti, A.; Noh, Y. Y. *ACS Appl. Mater. Interfaces* **2011**, *3*, 3205−3214.

(6) Fron, E.; Deres, A.; Rocha, S.; Zhou, G.; Mullen, K.; De Schryver, F. C.; Sliwa, M.; Uji-i, H.; Hofkens, J.; Vosch, T. *J. Phys. Chem. B* **2010**, *114*, 1277−1286.
(7) Strukelj, M.; Jordan, R. H.; Dodabalapur, A. *J. Am. Chem. Soc.* **1996**, *118*, 1213−1214.
(8) Suraru, S. L.; Zschieschang, U.; Klauk, H.; Wurthner, F. *Chem. Commun.* **2011**, *47*, 1767−1769.
(9) Lin, Y. Z.; Fan, H. J.; Li, Y. F.; Zhan, X. W. *Adv. Mater.* **2012**, *24*, 3087−3106.
(10) Ben-Sasson, A. J.; Chen, Z. H.; Facchetti, A.; Tessler, N. *Appl. Phys. Lett.* **2012**, *100*, 263306(1)−263306(4).
(11) Li, C. H.; Huang, C. H.; Kuo, M. Y. *Phys. Chem. Chem. Phys.* **2011**, *13*, 11148−11155.
(12) Letizia, J. A.; Salata, M. R.; Tribout, C. M.; Facchetti, A.; Ratner, M. A.; Marks, T. J. *J. Am. Chem. Soc.* **2008**, *130*, 9679−9694.
(13) Anthony, J. E.; Facchetti, A.; Heeney, M.; Marder, S. R.; Zhan, X. W. *Adv. Mater.* **2010**, *22*, 3876−3892.
(14) Alvey, P. M.; Ono, R. J.; Bielawski, C. W.; Iverson, B. L. *Macromolecules* **2013**, *46*, 718−726.
(15) Yuan, M. J.; Durban, M. M.; Kazarinoff, P. D.; Zeigler, D. F.; Rice, A. H.; Segawa, Y.; Luscombe, C. K. *J. Polym. Sci., Polym. Chem.* **2013**, *51*, 4061−4069.
(16) De Witte, P. A. J.; Hernando, J.; Neuteboom, E. E.; van Dijk, E. M. H. P.; Meskers, S. C. J.; Janssen, R. A. J.; van Hulst, N. F.; Nolte, R. J. M.; Garcia-Parajo, M. F.; Rowan, A. E. *J. Phys. Chem. B* **2006**, *110*, 7803−7812.
(17) Neuteboom, E. E.; Meskers, S. C. J.; van Hal, P. A.; van Duren, J. K. J.; Meijer, E. W.; Janssen, R. A. J.; Dupin, H.; Pourtois, G.; Cornil, J.; Lazzaroni, R.; Bredas, J. L.; Beljonne, D. *J. Am. Chem. Soc.* **2003**, *125*, 8625−8638.
(18) Kola, S.; Kim, J. H.; Ireland, R.; Yeh, M. L.; Smith, K.; Guo, W. M.; Katz, H. E. *ACS Macro Lett.* **2013**, *2*, 664−669.
(19) Zheng, Q. D.; Huang, J.; Sarjeant, A.; Katz, H. E. *J. Am. Chem. Soc.* **2008**, *130*, 14410−14411.
(20) Zhan, X. W.; Facchetti, A.; Barlow, S.; Marks, T. J.; Ratner, M. A.; Wasielewski, M. R.; Marder, S. R. *Adv. Mater.* **2011**, *23*, 268−284.
(21) Langhals, H. *Heterocycles* **1995**, *40*, 477−500.
(22) Choi, D.; Jeong, B. S.; Ahn, B.; Chung, D. S.; Lim, K.; Kim, S. H.; Park, S. U.; Ree, M.; Ko, J.; Park, C. E. *ACS Appl. Mater. Interfaces* **2012**, *4*, 702−706.
(23) Li, C.; Wonneberger, H. *Adv. Mater.* **2012**, *24*, 613−636.
(24) Bhosale, S. V.; Jani, C. H.; Langford, S. J. *Chem. Soc. Rev.* **2008**, *37*, 331−342.
(25) Polander, L. E.; Romanov, A. S.; Barlow, S.; Hwang, D. K.; Kippelen, B.; Timofeeva, T. V.; Marder, S. R. *Org. Lett.* **2012**, *14*, 918−921.
(26) Yan, Q. F.; Zhao, D. H. *Org. Lett.* **2009**, *11*, 3426−3429.
(27) Babel, A.; Jenekhe, S. A. *J. Am. Chem. Soc.* **2003**, *125*, 13656−13657.
(28) Yuan, Z. Y.; Xiao, Y.; Yang, Y.; Xiong, T. *Macromolecules* **2011**, *44*, 1788−1791.
(29) Guo, X. G.; Watson, M. D. *Org. Lett.* **2008**, *10*, 5333−5336.
(30) Hu, X. L.; Zuo, L. J.; Pan, H. B.; Hao, F.; Pan, J. Y.; Fu, L.; Shi, M. M.; Chen, H. Z. *Sol. Ener. Mater. Sol. Cells* **2012**, *103*, 157−163.
(31) Chen, Z. H.; Zheng, Y.; Yan, H.; Facchetti, A. *J. Am. Chem. Soc.* **2009**, *131*, 8−9.
(32) Zhan, X. W.; Tan, Z. A.; Domercq, B.; An, Z. S.; Zhang, X.; Barlow, S.; Li, Y. F.; Zhu, D. B.; Kippelen, B.; Marder, S. R. *J. Am. Chem. Soc.* **2007**, *129*, 7246−7247.
(33) Zhou, W. Y.; Wen, Y. G.; Ma, L. C.; Liu, Y. Q.; Zhan, X. W. *Macromolecules* **2012**, *45*, 4115−4121.
(34) Zhang, S. M.; Wen, Y. G.; Zhou, W. Y.; Guo, Y. L.; Ma, L. C.; Zhao, X. G.; Zhao, Z.; Barlow, S.; Marder, S. R.; Liu, Y. Q.; Zhan, X. W. *J. Polym. Sci., Polym. Chem.* **2013**, *51*, 1550−1558.
(35) Kim, Y.; Hong, J.; Oh, J. H.; Yang, C. *Chem. Mater.* **2013**, *25*, 3251−3259.
(36) Yan, H.; Chen, Z. H.; Zheng, Y.; Newman, C.; Quinn, J. R.; Dotz, F.; Kastler, M.; Facchetti, A. *Nature* **2009**, *457*, 679−686.
(37) Kim, R.; Amegadze, P. S. K.; Kang, I.; Yun, H. J.; Noh, Y. Y.; Kwon, S. K.; Kim, Y. H. *Adv. Funct. Mater.* **2013**, *23*, 5719−5727.
(38) Zhao, X. G.; Ma, L. C.; Zhang, L.; Wen, Y. G.; Chen, J. M.; Shuai, Z. G.; Liu, Y. Q.; Zhan, X. W. *Macromolecules* **2013**, *46*, 2152−2158.
(39) Kim, B. G.; Jeong, E. J.; Chung, J. W.; Seo, S.; Koo, B.; Kim, J. S. *Nat. Mater.* **2013**, *12*, 659−664.
(40) Kolhe, N. B.; Asha, S. K.; Senanayak, S. P.; Narayan, K. S. *J. Phys. Chem. B* **2010**, *114*, 16694−16704.
(41) Chaignon, F.; Falkenstrom, M.; Karlsson, S.; Blart, E.; Odobel, F.; Hammarstrom, L. *Chem. Commun.* **2007**, 64−66.
(42) Balakrishnan, K.; Datar, A.; Oitker, R.; Chen, H.; Zuo, J. M.; Zang, L. *J. Am. Chem. Soc.* **2005**, *127*, 10496−10497.
(43) Noriega, R.; Rivnay, J.; Vandewal, K.; Koch, F. P. V.; Stingelin, N.; Smith, P.; Toney, M. F.; Salleo, A. *Nat. Mater.* **2013**, *12*, 1037−1043.
(44) Pati, P. B.; Senanayak, S. P.; Narayan, K. S.; Zade, S. S. *ACS Appl. Mater. Interfaces* **2013**, *5*, 12460−12468.
(45) Senanayak, S. P.; Narayan, K. S. *Adv. Funct. Mater.* **2014**, *24*, 3324−3331.
(46) Rivnay, J.; Toney, M. F.; Zheng, Y.; Kauvar, I. V.; Chen, Z. H.; Wagner, V.; Facchetti, A.; Salleo, A. *Adv. Mater.* **2010**, *22*, 4359−4363.
(47) Li, J.; Zhao, Y.; Tan, H. S.; Guo, Y. L.; Di, C. A.; Yu, G.; Liu, Y. Q.; Lin, M.; Lim, S. H.; Zhou, Y. H.; Su, H. B.; Ong, B. S. *Sci. Rep.* **2012**, *2*, 1−9.